Nanotechnology

Load and release of gambogic acid via dual-target ellipsoidal-Fe3O4@SiO2@mSiO2-C18@dopamine hydrochloride -graphene quantum dots-folic acid and its inhibition to VX2 tumor cells

AUTHOR SUBMITTED MANUSCRIPT - NANO-132982.R3
Accepted Manuscript
Version of record at: https://doi.org/10.1088/1361-6528/aca76f

Load and release of gambogic acid via dual-target ellipsoidal-Fe_3O_4@SiO_2@mSiO_2-C_{18}@dopamine hydrochloride -graphene quantum dots-folic acid and its inhibition to VX2 tumor cells

Mengyang Dong[#a], Wenwen Liu[#a], Yuxiang Yang[a,b*], Meng Xie[c], Hongming Yuan[d], Chaoying Ni[b *]

[a]*School of Chemistry and Molecular Engineering, East China University of Science & Technology, Shanghai 200237, China.*

[b]*Department of Materials Science and Engineering, University of Delaware, Newark, Delaware 19716, United States*

[c]*School of Pharmacy, Jiangsu University, Zhenjiang212013, China.*

[d]*State Key Laboratory of Inorganic Synthesis and Preparative Chemistry, Jilin University, Changchun 130012, China.*

[#]Mengyang Dong and Wenwen Liu contributed equally to this work

**Corresponding author: yxyang@ecust.edu.cn, cni@udel.edu*

Abstract: Ellipsoidal-Fe_3O_4@SiO_2@mSiO_2-C_{18}@dopamine hydrochloride-graphene quantum dots-folic acid (ellipsoidal-HMNPs@PDA-GQDs-FA), a dual-functional drug carrier, was stepwise constructed. The α-Fe_2O_3 ellipsoidal nanoparticles were prepared by a hydrothermal method, and then coated with SiO_2 by Stöber method. The resulting core-shell structure, Fe_3O_4@SiO_2@mSiO_2-C_{18} magnetic nano hollow spheres, abbreviated as HMNPs, was finally grafted with graphene quantum dots

Accepted Manuscript
Version of record at: https://doi.org/10.1088/1361-6528/aca76f

(GQDs), dopamine hydrochloride (PDA) and folic acid (FA) by amide reaction to finally obtain HMNPs@PDA-GQDs-FA. Transmission electron microscopy (TEM), Fourier transform infrared spectroscopy (FTIR), fluorescence spectroscopy and element analysis proved the successful construction of the HMNPs@PDA-GQDs-FA nanoscale carrier-cargo composite. The carrier HMNPs@PDA-GQDs-FA has higher load (51.63±1.53%) and release (38.56±1.95%) capacity for Gambogic acid (GA). Cytotoxicity test showed that the cell survival rate was above 95%, suggesting the cytotoxicity of the carrier-cargo was very low. The cell lethality (74.91±1.2%) is greatly improved after loading GA because of the magnetic targeting of HMNPs, the targeting performance of FA to tumor cells, and the pH response to the surrounding environment of tumor cells of PDA. All results showed that HMNPs@PDA-GQDs-FA had good biocompatibility and could be used in the treatment of VX2 tumor cells after loading GA.

Keywords: Magnetic nanoparticles; Fluorescent graphene quantum dots; Targeting; Cytotoxicity

1. Introduction

Chemotherapy[1-3], radiotherapy [4-6] and surgical treatment [7] are widely used in cancer treatments in modern medicine. However, these methods can cause different degrees of damage to the normal function of human body. Therefore, it is essential to develop drug carriers to transport drugs and medicine and enhance targeted cancer therapies. In 1979, Couvreur, P. et al.[8] synthesized polyalkyl cyanoacrylate nanoparticles capable of drug loading and transport. At that time, it was a new

AUTHOR SUBMITTED MANUSCRIPT - NANO-132982.R3
Accepted Manuscript
Version of record at: https://doi.org/10.1088/1361-6528/aca76f

intracellular drug delivery system, which was ultrafine and metabolizable, yet the delivery vehicle could be associated with various drugs in a non-specific manner and degraded in vitro. With further developments of nano-loading systems, magnetic mesoporous materials gradually entered the field. Mesoporous silicon oxide has large specific surface area and highly ordered pore structure network, which combined with magnetic materials, can perform as drug loading composite systems. Avedian, N. et al.[9] prepared a tumor-target drug nanocarrier based on magnetic mesoporous silica nanoparticles (MMSNs) with Fe_3O_4 in the core, and polyimide-conjugated folic acid as the pH responsive shell. Erlotinib was loaded as a model responsive anticancer drug, and the release characteristics were evaluated at pH of 5.5 and 7.4, respectively, within 4 days. The release of erlotinib increased to 63±2.03% at lower pH values compared to 33±1.86% at normal pH values. The MMSNs loading of erlotinib inhibited the proliferation of HeLa cell lines. In addition, with iron compounds in the core, a mesoporous silica shell can function as a drug carrier for a variety of purposes, such as specific responses to temperature, pH and so on.

Blanco E [10] of the Methodist Hospital Research Institute in Houston, the United States, believes that the geometric morphology of nanoparticles affects hemorheology dynamics, cellular uptake and biodistribution in vivo. Non-spherical nanoparticles are more likely to roll and vibrate in the vascular system, greatly increasing the tendency of nanoparticles to contact the cell wall and the possibility of extravasation from blood vessels, which is conducive to the killing effect of nanoparticles to tumor cells [10]. Non spherical nanoparticles have different aspect ratios [11] and play an important

Accepted Manuscript
Version of record at: https://doi.org/10.1088/1361-6528/aca76f

role in the uptake of specific organs[12]. For example, because of the enhanced permeability and retention effect (EPR) of tumor cells, worm-like, rod-like, nanowire-like and peanut-like Fe_3O_4 nanoparticles are more easily absorbed by tumor cells [13, 11], strengthening the tumor treatment effect.

Oval nanoparticles are gradually favored by researchers in the field of biomedicine because of their most effective particle attachment and lowest in vitro internalization rate[14]. Unlike spherical nanoparticles, elliptical nanoparticles tumble and rotate under torsional stress, which increases the lateral drift of nanoparticles towards blood vessels in the microenvironment and can be used in the flow classification system for high-throughput particle separation, leading to the nanoparticles with desired shape being more conducive to be up-taken by cells. Non spherical nanoparticles are different from spherical nanoparticles in terms of endocytosis, intracellular retention, and internal circulation time [15]. Slender nanoparticles show superior pharmacokinetic characteristics and can reduce the uptake of drug carrier system by non-specific cells [16]. In addition, elliptical nanoparticles have higher surface area to volume ratio, which is conducive to loading more drugs.

Gambogic acid (GA), as a pure natural Chinese herbal medicine, has low toxicity. Tumor cells are not easy to develop drug resistance to GA, and it leaves behind little residue in the body after the treatment. The effective anticancer activity (in vitro and in vivo) of GA is mainly attributed to its down-regulation of telomerase activity to activate the damaged apoptotic pathway in cancer cells [17-19], which can inhibit the

AUTHOR SUBMITTED MANUSCRIPT - NANO-132982.R3
Accepted Manuscript
Version of record at: https://doi.org/10.1088/1361-6528/aca76f

growth of liver cancer, lung cancer, gastric cancer and breast cancer cells. Guo et al[17] studied the inhibitory effect of fusiformic acid (GA) on hepatoma cells SMMC-7721. MTT test (3-(4,5-dimethylthiazol-2-yl)-2,5-diphenyltetrazolium bromide)[20] results showed that GA demonstrated obvious cytotoxicity to SMMC-7721 cells at a concentration of 0.625-5.0 mg/L. When the concentration of GA reached 2 mg/L, the morphology of SMMC-7721 cells changed significantly, and the telomerase activity of SMMC-7721 cells was inhibited. Therefore, the clinical application of GA should be further studied in terms of anticancer activity, drug delivery and combined therapy[21].

Drug delivery systems have been visualized using organic fluorophores and semiconductor quantum dots to understand the cellular uptake [22]. However, the fluorescence of organic dyes, such as rhodamine B and fluorescein isothiocyanate, is significantly quenched by GO after conjugation [23,24]. The large size and heavy metal components of semiconductor quantum dots can alter the function of drug delivery systems. Thus, it is desirable to develop a functional luminescent nanosystem that can perform imaging and drug delivery tasks without the need for external dyes.

In this study, the HMNPs functionalized with graphene quantum dots (GQDs) are employed as a novel drug carrier, which have small size and tunable photoluminescence in addition to the remarkable physicochemical properties of GO. Dual-targeting pH-responsive HMNPs@PDA-GQDs-FA mesoporous nanocomposites were developed as the carrier to load anticancer drugs. HMNPs was loaded with the drug encapsulated with PDA, and then its surface was grafted with GQDs and FA.

Accepted Manuscript
Version of record at: https://doi.org/10.1088/1361-6528/aca76f

The system shows excellent drug-loading, sustained release and low cytotoxicity. During the polymerization, PDA continuously coats any material by the strong binding affinity of catechol functional groups to form the core-shell nanostructure[25]. The PDA layer thickness can be tuned via varying the dopamine concentration[26,27]. The encapsulation of PDA helps to enhance the pH response of the carrier to the surrounding environment of tumor cells. The introduction of FA enhances the targeting capability of the composite nanoparticles. Fluorescent GQDs were synthesized and conjugated with folic acid (FA) to demonstrate highly selective and specific tumor cell imaging. The FA-conjugated GQDs were then employed as a carrier of the antitumor drug Gambogic acid (GA) for targeted cell delivery[28]. Cytotoxicity shows that the composite carrier itself has no obvious toxicity. After loading GA, the drug system exhibits excellent anti-tumor effects.

2. Experimental section

2.1 Experimental materials and instruments

The materials used in this research include the following: citric acid, naphthenic acid, isooctyl alcohol, ferric sulfate, polyoxyethylene (5) nonylphenyl ether (Igepal CO-520), tetraethyl silicate (TEOS), octadecyl trimethoxysilane (C_{18}TMS), (3-aminopropyl) triethoxysilane (APTES), EDC, NHS, dimethyl sulfoxide (DMSO), folic acid (FA) (all of the above are from National Pharmaceutical Group Chemical Reagent Co., Ltd.), gambogic acid (GA) (Nanjing Jingzhu Biotechnology Co., Ltd.), PBS phosphate buffer (Wuhan Dr. Bioengineering Co., Ltd.), MTT (Sigma-Aldrich, USA), RPMI- 1640 medium (Invitrogen, USA), embryonic bovine serum (Hyclone,

AUTHOR SUBMITTED MANUSCRIPT - NANO-132982.R3
Accepted Manuscript
Version of record at: https://doi.org/10.1088/1361-6528/aca76f

USA), and sodium perrhenate injection (customized by Changhai Hospital, China). All chemicals were of analytical-reagent grade and used without further purification.

A Tecnai-12 transmission electron microscope (TEM) operating at 120 kV was used to characterize the particle morphology and size. The hydration diameter of the nanoparticles was measured by a laser scattering particle size analyzer. D/max 2550 VB/PC type X-ray diffractometer (K_α line of copper target, λ=0.15406 nm) was used for measurement at room temperature. Magna-IR 550 infrared spectrometer was used for collecting FTIR spectra. VSM BHS-55 vibrating sample magnetometer was used to determine the magnetic properties of the sample. Shimadzu UV-2450 spectrophotometer was used to determine the ultraviolet-visible absorption spectra.

2.2 Ethical statement

The study was approved by the School of Pharmacy, Jiangsu University, Zhenjiang 212013, China.

2.3 Preparation of α-Fe_2O_3@SiO_2

The preparation of GQDs and α-Fe_2O_3 are described in detail in the supporting Information.

Afterwards, 0.5 g Igepal CO-520 was added with 11mL of cyclohexane and dispersed evenly with an ultrasonic oscillator. 1.25 mg dry α-Fe_2O_3 and 0.2 mL ammonia water were added to the mixture solution under stirring. Finally, 0.28 mL TEOS was added slowly.

2.4 Preparation of nano hollow spherical Fe_3O_4@SiO_2@mSiO_2-C_{18} (HMNPs)

2mL of boiling cooled deionized water, 10 mL ethanol and 0.72 mL ammonia

Accepted Manuscript
Version of record at: https://doi.org/10.1088/1361-6528/aca76f

were added to a flask with 5 mL α-Fe_2O_3@SiO_2(0.05g) anhydrous ethanol solution. Then, 0.3mL of C_{18}TMS/TEOS solution was added slowly. The mixed solution reacted at 25ºC for 6h, and α-Fe_2O_3@SiO_2@mSiO_2-C_{18} was obtained by centrifugation. (Note: Preparation of C_{18}TMS/TEOS solution: 1mL C_{18}TMS dissolved at 2.47mL TEOS).

0.05 g α-Fe_2O_3@SiO_2@mSiO_2-C_{18} was added with 28 mL of boiled and cooled deionized water and 2mL anhydrous ethanol, and the mixture was dispersed evenly with ultrasonic oscillator. The reaction was carried out at 130ºC for 20 hours in a high-pressure reactor of PTFE to change the polysiloxane with α-Fe_2O_3@SiO_2@mSiO_2-C_{18} shell structure from low to high poly state. After the reaction, the product was separated by centrifugation, and then dried in vacuum for 6 hours. The quartz boat containing dry products was put into a tube furnace and calcined at 550ºC for 6 h to form an outer pore under nitrogen atmosphere. Then, hydrogen and nitrogen (H_2(4%)/N_2) were inlet simultaneously and the products in the furnace was calcined at 400ºC for 3 h to obtain Fe_3O_4@SiO_2@mSiO_2-C_{18} magnetic nano hollow spheres, *i.e.* the HMNPs.

The preparation of HMNPs-GQDs is described in the supporting Information.

2.5 Drug loading

0.04 g GA was dissolved in DMSO and then, the solution was made up to volume with a 20 mL volumetric flask. 20 mL, 10 mL, 6 mL, 5 mL, and 4 mL of the above solution were made up to volume with 20 mL, respectively. 10 mg HMNPs was dispersed uniformly by ultrasound in 20 mL inactivated fetal bovine serum

AUTHOR SUBMITTED MANUSCRIPT - NANO-132982.R3
Accepted Manuscript
Version of record at: https://doi.org/10.1088/1361-6528/aca76f

RPMI-1640 culture medium, and then 20 mL above prepared different concentration GA solution was added and shaken at 4 °C for 48 hours. The product was separated by centrifuge, and then the supernatant was taken to measure the absorbance.

2.6 Preparation of HMNPs@PDA-GQDs-FA and GA loaded HMNPs@PDA-GQDs-FA

20 mg HMNPs (GA loaded or unloaded) was dispersed with ultrasonic in 50 mL Tris buffer solution (pH=8.5~10 mM), and then, dopamine hydrochloric acid solution was slowly dropped into mixed solution while stirring. Centrifugal washing with deionized water was carried out after 6 hours of reaction, and the GA-HMNPs@PDA was obtained after freeze-dried for 24 hours. 5 mL GQDs solution (0.1 mg/ml) was diluted to 20 mL with deionized water and then oscillated at 37°C for 2 hours after adding EDC (10 mg), NHS (8 mg) in turn. 20 mg GA-HMNPs@PDA was added and reacted for 2 h to graft GQDs onto the GA-HMNPs@PDA surface. FA (50 mg) and NHS (80 mg) were dissolved in 10 mL MES buffer solution and stirred for 30 min, and the black solid was obtained by magnetic separation. The sample was re-dispersed in PBS buffer solution, stirred overnight in the dark, separated magnetically, and lyophilized for 24 hours to obtain GA-HMNPs@PDA-GQDs-FA.

2.7 Suspension test

Suspension experiments of GA-HMNPs@PDA-GQDs-FA nanoparticles is described in the supporting Information.

2.8 Drug sustained release

10 mg of GA-HMNPs@PDA-GQDs-FA loaded with the drug was dispersed in

Accepted Manuscript
Version of record at: https://doi.org/10.1088/1361-6528/aca76f

25 mL phosphoric acid buffer solution (pH=7.4 and pH=5.7) by ultrasound, and then, oscillated continuously at 37°C. The absorbance was measured at set intervals after centrifugation and the same pH value of phosphoric acid buffer solution was added.

2.9 Cytotoxicity test

Cytotoxicity experiments of all sample compounds were detected by MTT method. The VX2 cells in good condition were evenly spread into 96 hole plate, and then cultured in 5% CO_2、37°C incubator. When the cells were attached to the wall and the density was about 80%, the supernatant was discarded. HMNPs-GQDs, HMNPs@PDA-GQDs, HMNPs@PDA-GQDs-FA (with concentration per sample at 0、25、50、75、100 and 125 μg/mL, respectively) were incubated with VX2 cells for 24 hours in a 5% CO_2、37°C atmosphere, respectively. After incubation, the remaining solution in each hole was removed and rinsed with PBS buffer solution. The background value was measured with an enzyme marker, and then the MTT solution was added to the orifice plate. After incubation in the incubator for 4 hours, the MTT residue was removed and dimethyl sulfoxide was added to dissolve the crystallization. Finally, the absorbance values were measured by enzyme labeling at the wavelength of 570 nm and the cell survival rate was calculated:

$$\text{Cell viability}(\%) = \frac{\text{ODexperimental} - \text{ODblank}}{\text{ODtumor} - \text{ODblank}} \times 100\%$$

The $OD_{experiment}$ is the absorbance value of the sample, the OD_{blank} is the absorbance value of the culture medium and the MTT, and the OD_{tumor} is the absorbance value of the cell only.

2.10 Laser confocal photographing

AUTHOR SUBMITTED MANUSCRIPT - NANO-132982.R3
Accepted Manuscript
Version of record at: https://doi.org/10.1088/1361-6528/aca76f

Spread MCF-7 and VX2 cells evenly onto a 96-well plate, cultured at 5% CO_2、37°C, aspirated the remaining culture medium when the cells grew to about 80% density. Then, HMNPs@PDA-GQDs and HMNPs@PDA-GQDs-FA were added and fixed with 4% paraformaldehyde for 20 minutes, cellular up-taken for 2 hours, and dyed nucleus with 1μg/mL DAPI for 20 minutes. For each substance added, the residual solution was discarded and washed with PBS for 2-3 times. Finally, a drop of anti-fluorescence quencher was added and observed under laser confocal microscope.

2.11 Determination of Biodistribution in the Mice

Female healthy mice were subjected to injection with $^{99}Tc^{m}$ labeled HMNPs@PDA-GQDs-FA via tail vein (0.1 mL of 0.1 mCi per mouse, at a dose of 10 mg). The mice were then sacrificed at 60 min after injection. Blood, heart, lung, kidney, liver, spleen, pancreas, bravery, small intestine, large intestine, brain and skeleton were collected for counting of radioactivity, and the amount of $^{99}Tc^{m}$ labeling in these thirteen collected organs was determined by gamma counter, respectively. In the experimental process, the liver and spleen from the mice were exposed to targeting gradient pulsed magnetic field under adequate magnetic field strength[29].

2.12 Statistical analysis

The significant difference of each trait from GA loading and PH on the cumulative drug release rate was analyzed by one-way Analysis of Variance (ANOVA) followed by Tukey’s multiple comparisons. Difference at $P < 0.05$ or $F > Fcrit$ was significant. The figures were drawn using OriginPro 8.5 and Photoshop CS6.

3. Result and discussion

3.1 Structural characterization of the composite nanoparticles

As shown in the upper right corner of Fig. 1(a), α-Fe_2O_3 microspheres with a

Accepted Manuscript
Version of record at: https://doi.org/10.1088/1361-6528/aca76f

length of about 80 nm and a width of 40 nm are uniformly dispersed. The silica coating shell is around 6 nm, shown in Fig. 1(a) and (b). Fe_2O_3@SiO_2@mSiO_2-C_{18} is obtained by re-coating with C_{18}TMS and TEOS, as shown in Fig. 1(c). The thickness of the shell is about 18 nm and the cavity gap between the core and the shell is about 2.5 nm. After calcination in H_2 and N_2, the particle size does not change a lot and is mostly between 120 nm-150 nm. Fig. 1(d) shows a HRTEM image of SiO_2 shell and α-Fe_2O_3. The shell has a very regular arrangement of parallel channels and a rough measurement of some parallel channels in the diagram shows that the pore center spacing is about 2.9 nm, corresponding to the mesoporous SiO_2 synthesized by octadecyl trimethoxysilane C_{18}TMS as template in the literature[30]. There are well-defined lattice fringes observed from HRTEM micrograph recorded in the lower right corner of Fig. 1(d). It can be seen that the interplanar spacing of α-Fe_2O_3 is 0.25nm and the particle morphology demonstrates a polycrystalline characteristic.

AUTHOR SUBMITTED MANUSCRIPT - NANO-132982.R3
Accepted Manuscript
Version of record at: https://doi.org/10.1088/1361-6528/aca76f

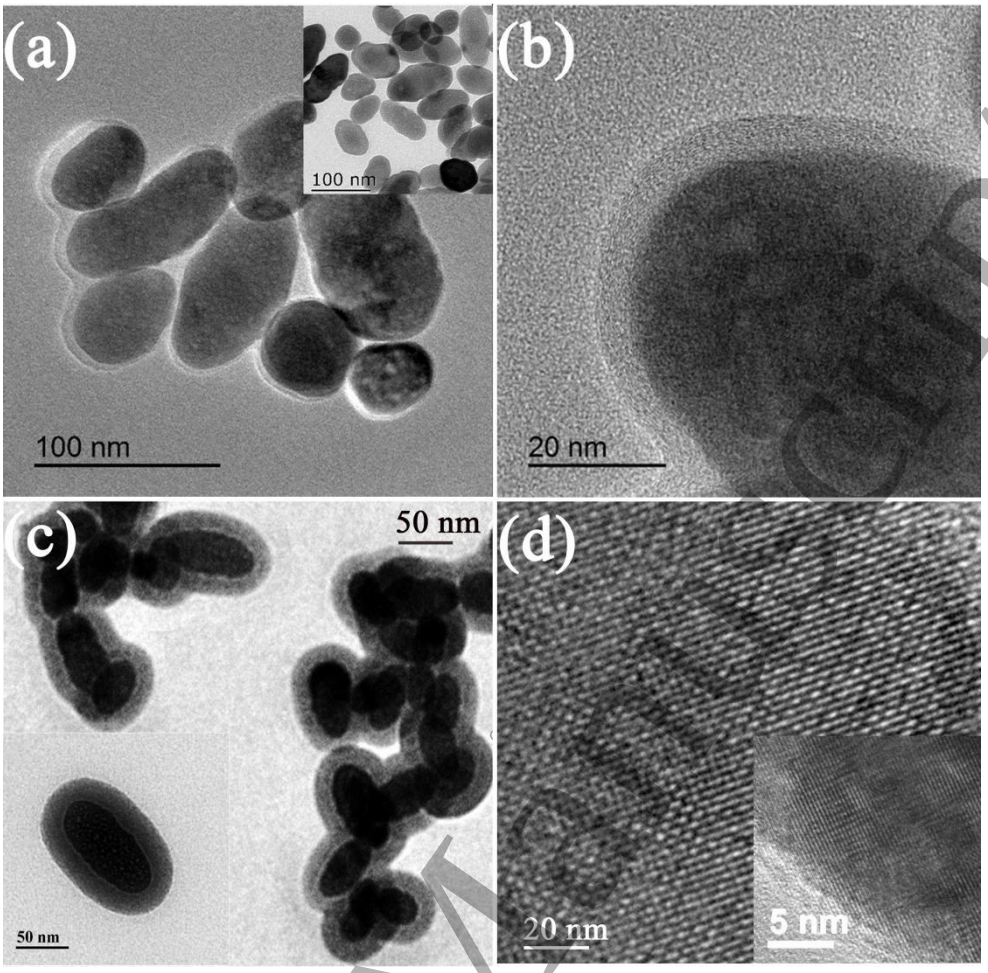

Fig. 1 TEM of (a,b) Fe_2O_3@SiO_2 ,(c) Fe_2O_3@SiO_2@mSiO_2-C_{18} and (d)HR-TEM of mSiO_2 and α-Fe_2O_3 (lower right corner)

SEM images of α-Fe_2O_3、Fe_2O_3@SiO_2 and Fe_2O_3@SiO_2 @SiO_2-C_{18} (HMNPs) are shown in Figure 2. It can be seen from Fig. 2 that oval α-Fe_2O_3 was successfully synthesized with smooth surface and good dispersion. The elliptical structure in Fig. 2b is rougher than that in Fig. 2a, because its surface is coated with SiO_2, indicating that Fe_2O_3@SiO_2 was successfully synthesized. Fig. 2c Fe_2O_3@SiO_2@SiO_2-C_{18} surface is much rougher because the grafting of SiO_2, SiO_2-C_{18}, etc., increases the surface roughness of particles, indicating that Fe_2O_3@SiO_2@SiO_2-C_{18} was also successfully synthesized.

Accepted Manuscript
Version of record at: https://doi.org/10.1088/1361-6528/aca76f

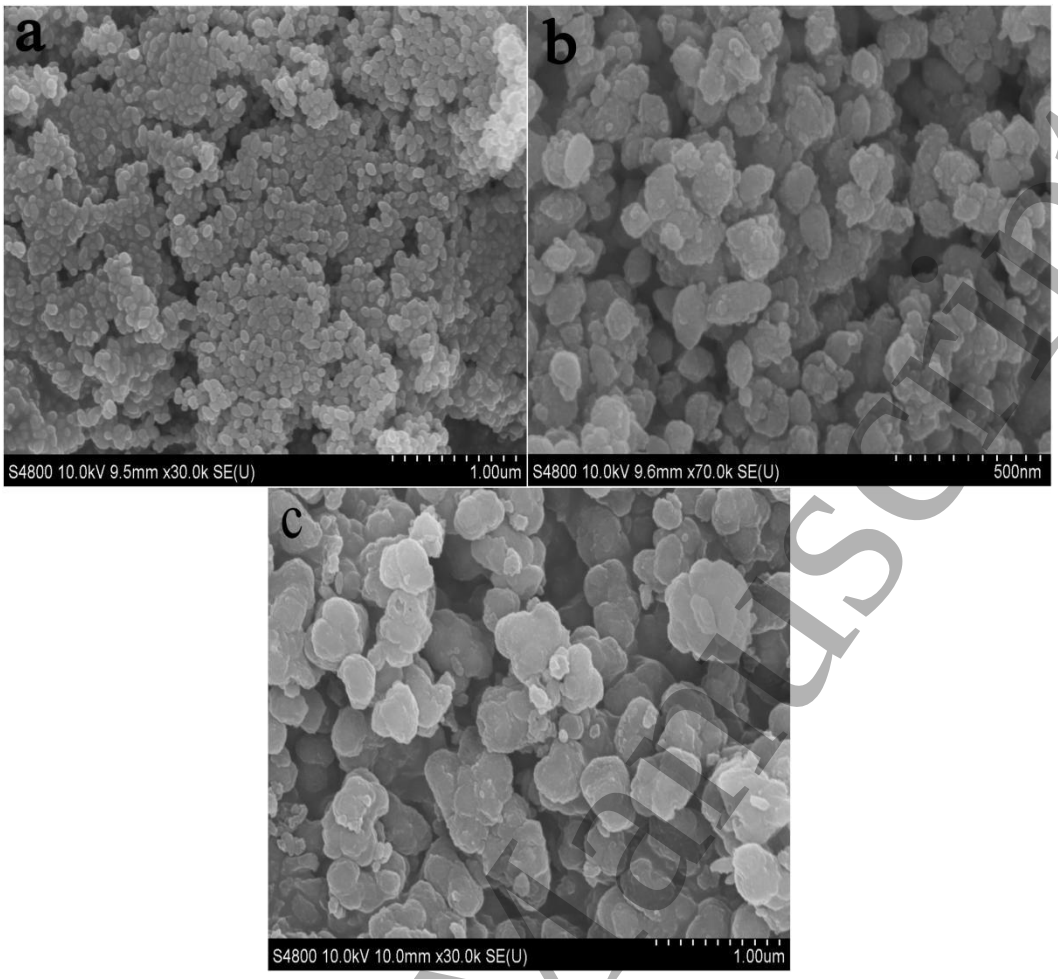

Fig. 2 SEM of (a) α-Fe_2O_3, (b)Fe_2O_3@SiO_2 ,(c) Fe_2O_3@SiO_2@mSiO_2-C_{18}

In order to study molecular structures and chemical bonds of HMNPs, Fourier infrared spectroscopy (FTIR) was used in this study. As shown in Fig. S1a, the Fe-O characteristic peak is shown at 582 cm^{-1}, which proves the existence of Fe_3O_4 in the HMNPs. The 3450 cm^{-1} wide band is shown in all infrared spectra, which belongs to OH stretching vibration. Two Si-O-Si-related bands were observed at 1105 cm^{-1} and 456 cm^{-1}, indicating the existence of SiO_2 shells on the surface of HMNPs. The stretching vibration of -CH was observed at 2933 cm^{-1}, indicating the conjugation of (3-aminopropyl) triethoxysilane (APTES) on the surface of HMNPs. New peaks at 1394 cm^{-1} after covalent binding with GQDs can be attributed to the C-N stretching of

AUTHOR SUBMITTED MANUSCRIPT - NANO-132982.R3
Accepted Manuscript
Version of record at: https://doi.org/10.1088/1361-6528/aca76f

the EDC/NHS. The other peak at 1584 cm^{-1} is attributed to the vibration of NH-CO-, which indicates the formation of an amide bond in the HMNPs-GQDs. Fig. S1b shows peaks at 1086 cm^{-1} and 967 cm^{-1}, which is attributed to the Si-O-Si stretching vibration and silanol vibration, respectively. The peak strengthening at 1636 cm^{-1} after encapsulation with PDA can be attributed to the aromatic ring framework stretching vibration, which confirms the presence of the PDA coating on the surface of HMNPs. The broad absorption peak at 3438 cm^{-1} can be attributed to the stretching vibration of N-H and O-H. As for HMNPs@PDA-GQDs-FA, new peaks appearing at 1504 cm^{-1} indicates the targeted ligand FA has been grafted onto the composite nanoparticles.

In order to study the relationship among GQDs, HMNPs, FA, PDA and HMNPs-GQDs, XPS analysis is carried out. As shown in Fig. 3a, all three composite nanoparticles have Si, C, N, and O. The Si2p peak intensity of the HMNPs@PDA-GQDs-FA is slightly less than that of the HMNPs@PDA, indicating the successful incorporation of FA. In Fig. 3d, compared to the HMNPs-GQDs, the obvious strengthening peak of N1s at the binding energy of 406 eV in the HMNPs@PDA and HMNPs@PDA-GQDs-FA indicates the presence of PDA layer. The peak mainly occurring at 285 eV is attributed to the existence of C-C or C-H (Fig.3b). The C1s peak is further divided (Fig. 3c) as the carbon atoms in the HMNPs-GQDs mainly exist in the form of three functional groups which are C-C peak at 285 eV, C-O peak at 286.6 eV and O=C-N peak at 288.7 eV.

Accepted Manuscript
Version of record at: https://doi.org/10.1088/1361-6528/aca76f

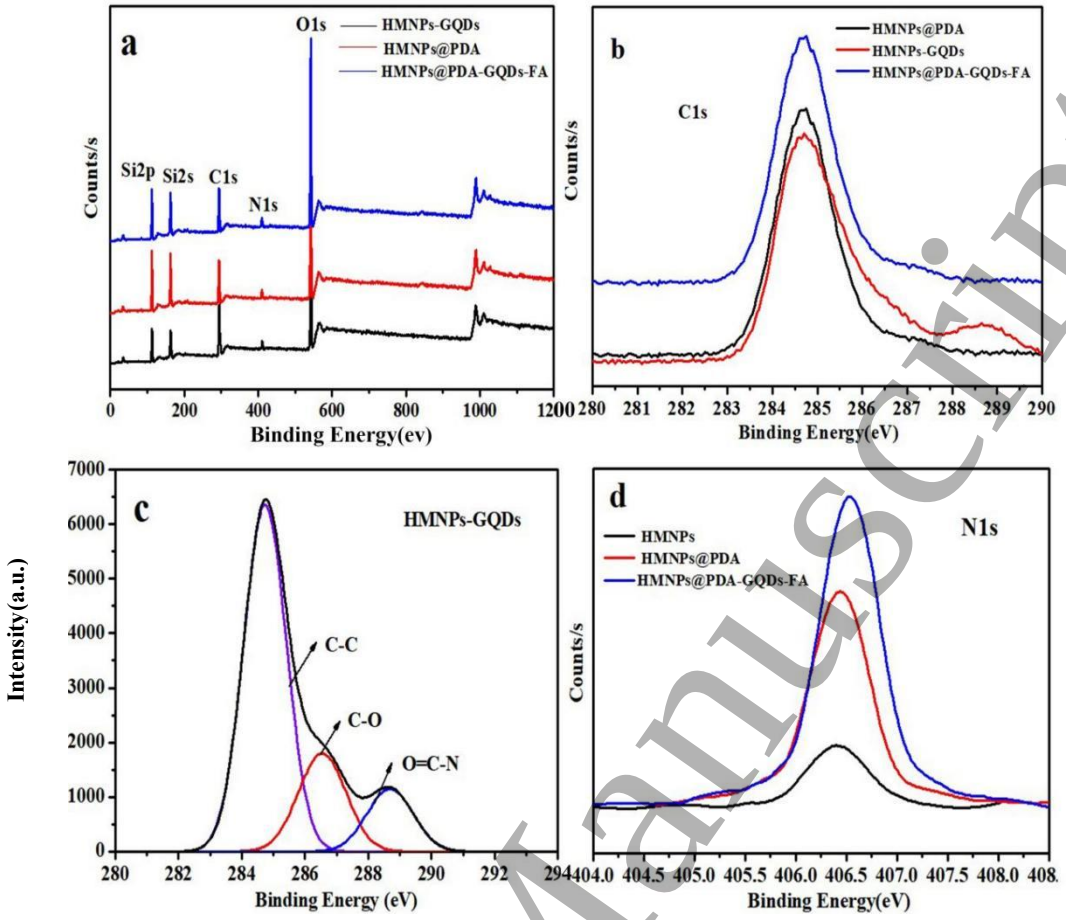

Fig. 3 (a) XPS spectrum of HMNPs-GQDs、HMNPs@PDA andHMNPs@PDA-GQDs; (b) C1s peaks of HMNPs-GQDs、HMNPs@PDA and HMNPs@PDA-GQDs; (c) C1s peaks of HMNPs-GQDs; (d) N1s peaks of HMNPs-GQDs、HMNPs@PDA and HMNPs@PDA-GQDs

The fluorescence spectra of HMNPs, HMNPs-GQDs, HMNPs@PDA-GQDs and HMNPs@PDA-GQDs-FA excited at the wavelength of 350 nm are shown in Fig. 4. The cases of GQDs aqueous solution under two different light sources are shown in upper right corner of Fig. 4. Under the sunlight, GQDs aqueous solution is yellow, while it shows green fluorescence under the ultraviolet lamp. GQDs has absorption peaks at 396 nm and HMNPs-GQDs has absorption peaks in the same position, but the fluorescence intensity is weaker. This can be explained that covalent bonds are formed between the amino group on HMNPs and the carboxyl group on GQDs, resulting in the transfer of electrons and energy, which leads to certain degree of

AUTHOR SUBMITTED MANUSCRIPT - NANO-132982.R3
Accepted Manuscript
Version of record at: https://doi.org/10.1088/1361-6528/aca76f

fluorescence quenching of GQDs. The peaks of HMNPs@PDA-GQDs and HMNPs@PDA-GQDs-FA are also at the same position and the fluorescence intensity does not decrease greatly after grafting FA. As a result, composite nanoparticles HMNPs@PDA-GQDs-FA have been successfully prepared and can be used for cell-labeled fluorescence imaging and tracing live cell life dynamic processes.

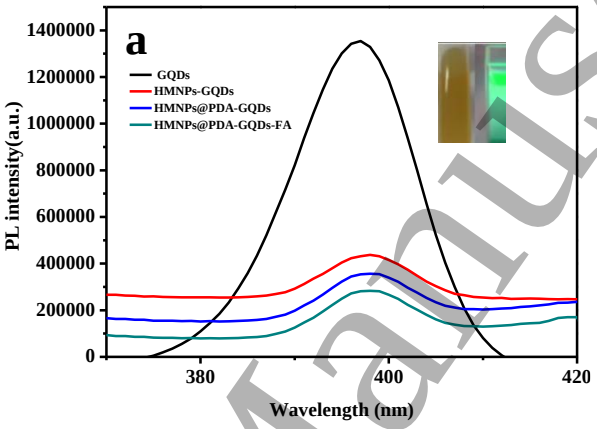

Fig. 4 Fluorescence spectra of GQDs、HMNPs-GQDs、HMNPs@PDA-GQDs and HMNPs@PDA-GQDs-FA

N_2 adsorption and desorption technology is employed to study the porosity of HMNPs@PDA-GQDs-FA. As shown in Fig. 5, composite nanoparticles HMNPs@PDA-GQDs-FA are mesoporous materials. The N_2 adsorption desorption isotherms in Fig. 5b shows that there are adsorption hysteresis loops in the high pressure region, which belong to the H4 type isotherms in the IUPAC. The pore size of the composite nanoparticles is mainly distributed in 2.53 nm and 5.81 nm, as shown in Fig. 5a, and among them, 2.53 nm has the strongest peak. The surface area is calculated using the Brunauer-Emmett-Teller (BET) method and the specific surface area and pore volume are shown in Table 1.

The above data suggest that the composite nanoparticles

Accepted Manuscript
Version of record at: https://doi.org/10.1088/1361-6528/aca76f

HMNPs@PDA-GQDs-FA are suitable for drug loading. The hysteresis loops of HMNPs、HMNPs-GQDs、HMNPs@PDA-GQDs and HMNPs@PDA-GQDs-FA were tested at room temperature and the magnetic properties of the nanomaterials were evaluated. Fig. 5c shows that the hysteresis loops are symmetrical and the coercivity is relatively small. The saturation magnetization M_s of the HMNPs is 26.96 emu/g and the residual magnetization is about 2.67 emu/g. The saturation magnetization M_s of HMNPs-GQDs is 26.81 emu/g and the residual magnetization is about 3.84 emu/g, which relatively decreases compared to HMNPs indicating GQDs are successfully grafted onto HMNPs surface. For the purpose of studying the magnetic properties of the composite nanoparticles, the hysteresis loop of HMNPs@PDA-GQDs was tested at room temperature. The hysteresis loop of the HMNPs@PDA-GQDs is S type with a relatively small coercivity and a saturation magnetization M_s 17.07 emu/g, and the residual magnetization is about 4.47 emu/g. The saturation magnetization M_s of HMNPs@PDA-GQDs-FA is 15.06 emu/g and the residual magnetization is about 5.32 emu/g. It can be seen from the above results that the grafted functional groups have little influence on the magnetic properties of the raw materials.

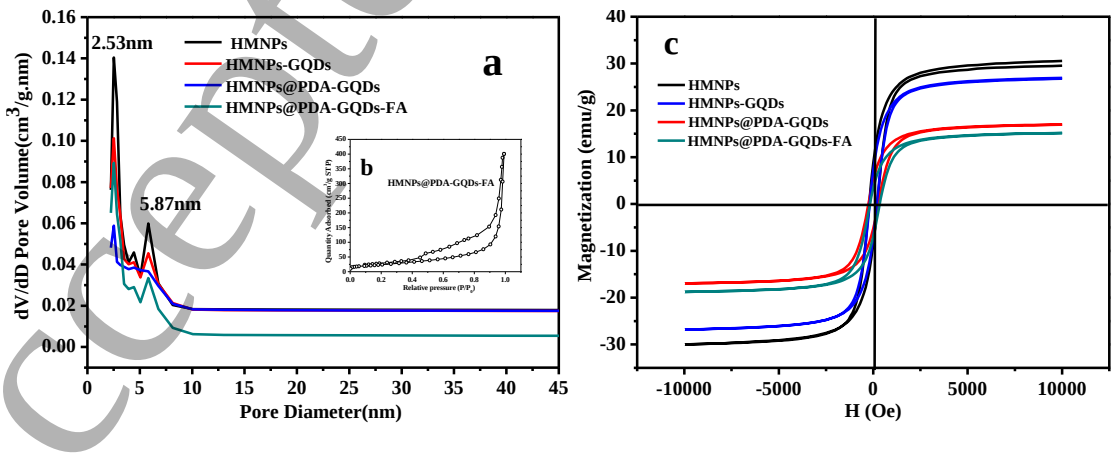

AUTHOR SUBMITTED MANUSCRIPT - NANO-132982.R3
Accepted Manuscript
Version of record at: https://doi.org/10.1088/1361-6528/aca76f

Fig. 5 (a) pore size distribution and Pore size distribution, (b) N_2 adsorption-desorption isotherm, and (c) Hysteresis loops

Table 1 BET related data

	BET surface area (m^2/g)	Pore volume (cm^3/g)	Pore size (nm)
HMNPs	111.78	0.71	2.53
HMNPs-GQDs	95.59	0.63	2.53
HMNPs@PDA-GQDs	64.31	0.48	2.52
HMNPs@PDA-GQDs-FA	60.29	0.41	2.45

In order to study the effect of surface modification and loaded drugs on the surface charge of composite mesoporous particles, zeta potential was measured at pH =7.4 as shown in Fig. 6. HMNPs-NH_2 is positively charged (21.56 mV) by the amino group on the surface. The zeta potential of HMNPs-GQDs (18.80 mV) which is less positive because of negatively charged of carboxyl group. The zeta potential of HMNPs@PDA-GQDs (20.20 mV) becomes more positive because of the amino group on the PDA. However, the carboxyl groups on FA and GA gradually reduced the Zeta potential of HMNPs@PDA-GQDs-FA and HMNPs@PDA-GQDs-FA(GA) to 10.1 mV and -7.00 mV, respectively. Positively charged HMNPs@PDA-GQDs-FA is more likely to penetrate anionic cell membranes and has good cell penetration, showing the feasibility of being used as drug carriers.

Accepted Manuscript
Version of record at: https://doi.org/10.1088/1361-6528/aca76f

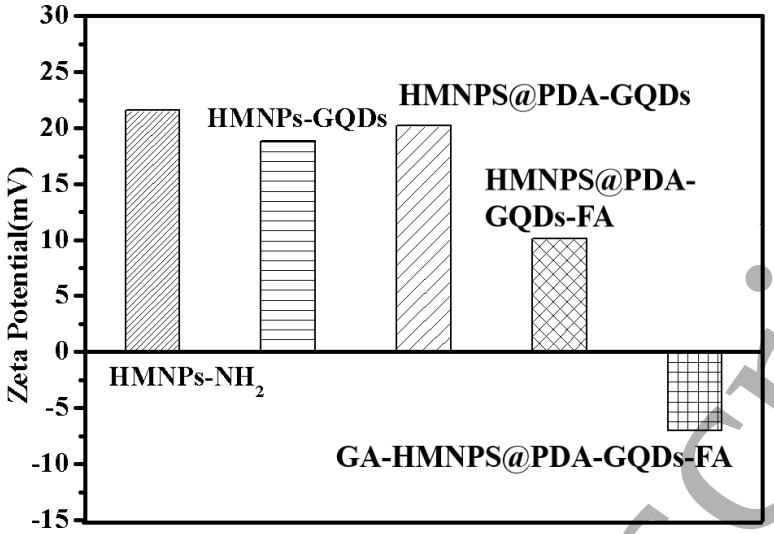

Fig. 6 Zeta-potentials of HMNPs-NH_2、HMNPs-GQDs、HMNPs-GQDs@PDA、HMNPs-GQDs@PDA-FA、and HMNPs-GQDs@PDA-FA(GA)

The changes in suspension rate for the HMNPs@PDA-GQDs-FA nanoparticles are shown in Fig. S2. In Figure 7, after 2 h periods of static placing duration, the suspension rate was retained for more than 90%; the suspension rates was retained for 75% after 8 h periods of static placing duration. As shown in Fig. S2, the suspension rate for the HMNPs@PDA-GQDs-FA nanoparticles was still retained at more than 55% after 20 h periods of static placing duration.

The reason for these results can be explained as follows: When the HMNPs@PDA-GQDs-FA nanoparticles was laid for periods of static placing duration, sedimentation would result in an increased concentration at the lower part of HMNPs@PDA-GQDs-FA nanoparticles and a decreased concentration at upper part of the HMNPs@PDA-GQDs-FA nanoparticles, and by virtue of the Brownian movement, the formed gradient concentration would lead to reversed diffusion.

3.2. Drug loading and sustained release

The highest loading efficiency and embedding efficiency of HMNPs@PDA-GQDs-FA reached 11.74±2.53% and 51.63±1.53% by addition of

AUTHOR SUBMITTED MANUSCRIPT - NANO-132982.R3
Accepted Manuscript
Version of record at: https://doi.org/10.1088/1361-6528/aca76f

1.0、1.6、2.4、4.0 and 8.0 mg of GA into 40 mL of 40 mM DMSO and inactivated fetal bovine serum RPMI-1640 culture medium with 10 mg HMNPs@PDA-GQDs-FA (Table 2). When GA dosage exceeded 4 mg, the loading amount began to become saturated, which can be explained that the adsorption capacity of mesoporous hollow spheres with definitive surface area and pore volume is limited, and when the surface adsorption layer reaches saturation, the excess drug molecules can only pile up to the second layer of the surface, preventing the drug loading. Therefore, the most suitable dosage of GA is 4 mg, and the drug encapsulation rate is 45.34±0.24% and the drug loading is 8.31±2.02%.

Table 2 HMNPs@PDA-GQDs-FA Load to GA

m_{GA}(mg)	$m_{Loading\text{-}GA}$(mg)	Embedding efficiency (%)	Loading efficiency(%)
1.0	0.4541±0.57	45.41±0.66	2.22±1.73
1.6	0.7659±0.12	47.87±1.30	3.68±1.19
2.4	1.2391±0.68	51.63±1.53	5.83±1.72
4.0	1.8136±0.44	45.34±0.24	8.31±2.02
8.0	2.6618±0.35	33.27±0.51	11.74±2.53

We used One-Way ANOVA analysis method to discuss and analyze the influence of GA loading and PH on the cumulative drug release rate. From Table 3. A, we can see that F>Fcrit, rejecting the original hypothesis, which shows that the amount of GA has an impact on the characteristic value of drug encapsulation rate. It can be seen from Table 3. B that its F>>Fcrit, rejecting the original hypothesis, indicates that PH has a more significant impact on the characteristic value of drug

Accepted Manuscript
Version of record at: https://doi.org/10.1088/1361-6528/aca76f

release rate, and PH has a greater impact on the cumulative drug release rate. It is proved that the magnetic nanoparticles encapsulated by PDA can achieve greater release in the slightly acidic environment of tumors, playing the role of pH controlled switch.

Table 3 Single factor ANOVA: GA load vs. PH HMNPs@PDA-GQDs-FA Effect of cumulative sustained release rate of carrier drugs

A) GA loading amount

Source	SS	df	MS	F	P-value	F crit
Between groups	568.8969	4	142.2242	148.6395	7.3271E-09	3.4780
Within group	9.5684	10	0.9568			
Total	578.4653	14				

B) PH

Source	SS	df	MS	F	P-value	F crit
Between groups	39.9900	1	39.9900	6875.0744	1.2681E-07	7.7086
Within group	0.0232	4	0.0058			
Total	40.0132	5				

The PDA film coated on the surface of HMNPs could block the pores and inhibit drug release. The PDA membrane encapsulated on the surface of HMNPs is a pH-dependent membrane that acts as a pH-controlled switch to control or inhibit the release of drugs. For the PDA-coated HMNPs (HMNPs@PDA-GQDs-FA), the drug release increases with increasing solution acidity.

To further explore pH dependence on sustained drug release of PDA, release of HMNPs@PDA-GQDs-FA is studied in pH 7.4 and 5.7 respectively. As shown in Fig. 7d, the cumulative release of GA by HMNPs@PDA-GQDs-FA is 33.39±2.13% at pH=7.4. When pH=5.7, the cumulative release of HMNPs@PDA-GQDs-FA to GA

AUTHOR SUBMITTED MANUSCRIPT - NANO-132982.R3
Accepted Manuscript
Version of record at: https://doi.org/10.1088/1361-6528/aca76f

increases to 38.56±1.95%, which indicates that the PDA film encapsulated on the HMNPs surface is a pH-dependent membrane acting as a pH controlled switch to control or inhibit drug release. Due to the acidic microenvironment of the tumor, this pH-dependent release behavior can enhance the therapeutic effect on cancer cells and minimize potential harm to normal cells.

Three kinetic models of drug release were employed to study the release kinetics mechanism of HMNPs@PDA-GQDs-FA in vitro, and the fitting was determined according to the R^2 of the fitting correlation coefficient.

The first is the Higuchi model: $Q_t = K_H t^{\frac{1}{2}}$, where Q_t is the cumulative release percentage of the drug at time t and K_H is the diffusion constant[31].

The second is a first-order kinetic model: $Q_t = Q_m[1 - exp(-kt)]$, where Q_t is the cumulative drug release at time t, Q_m the cumulative drug release at equilibrium, and the first order kinetic release constant is K[32].

A third is the Weibull dynamics model: $Q_t = Q_m[1 - exp(-at^b)]$, where Q_t is the cumulative release of drugs at time t, Q_m at equilibrium, and the a and b are constants[33].

On the basis of the sustained release data of the HMNPs@PDA-GQDs-FA, the Q_t is drawn by t, and three kinetic models are used to fit in Fig. 7. It can be seen that the drug release of the HMNPs@PDA-GQDs-FA does not conform to the Higuchi kinetic model from Fig. 7a, and the fitting correlation coefficient shows $R^2 = 0.7308$, which underestimates the time of rapid release of the drug, indicating that the release of the compound nanoparticles is not completely controlled by a diffusion process.

Accepted Manuscript
Version of record at: https://doi.org/10.1088/1361-6528/aca76f

When fitting the drug release data with the first-order kinetic model, the fitting correlation coefficient is R^2 = 0.8263 from Fig.7b. The first-order kinetic model underestimates the fast release stage of the GA and also overestimates the stable release amount of the GA. The Weibull kinetic model was used to simulate the GA slow release and the correlation coefficient was R^2 = 0.9825 from Fig.7c, which indicates that the HMNPs@PDA-GQDs-FA slow release is more in line with the Weibull kinetic model. According to this model, the dosage of compound nanoparticles HMNPs@PDA-GQDs-FA tumor cells can be designed. Drug release is divided into two stages. The initial release is due to the diffusion of the outer surface GA of the nanomaterials. The later stage of release is the slow diffusion of drug molecules from the hollow spheres through the mesopores into the external environment. Due to the resistance among the pore sizes and the environmental pressure difference between the inside and outside of the hollow sphere, the drug diffuses slowly and finally reaches an equilibrium. The release rate of drug molecules is then determined by the slower step. Bhaskar et al.[34] developed a simple procedure to establish whether the diffusion through the particle was the rate limiting step. For a particle diffusion-controlled release, Bhaskar et al.[34] obtained the following equation: $\ln(1 - x_t) = -1.59(6/d_p)^{1.3} D^{0.65} t^{0.65}$, where d_p is the diameter of the nanoparticles and D is the diffusivity. This suggests that particle diffusion control can be tested by simply testing the linearity between $-\log(1-Xt)$ and $t^{0.65}$. This method was applied to the experimental data, and a good linear relationship (correlation coefficient R^2 = 0.9872) is obtained for the release at pH 5.7 from Fig. 7e, indicating that the diffusion

AUTHOR SUBMITTED MANUSCRIPT - NANO-132982.R3
Accepted Manuscript
Version of record at: https://doi.org/10.1088/1361-6528/aca76f

through the particle is the rate limiting step[35]. In contrast, the relationship between $-\log(1-x_t)$ and $t^{0.65}$ is nonlinear at pH 7.4. It may be explained as follows: under acidic conditions, the drug molecules adsorbed on the outside of the hollow sphere diffuse outwards first, and the internal drug molecules will diffuse externally because the hollow sphere has the same charge as itself, and the two will repel each other. Under neutral conditions, the drugs loaded on the surface of the nanocarrier will be rapidly released, while the drugs loaded in the cavity will exist stably and only diffuse slowly through themselves. Hence, the graph of $-\log(1-x_t)$ vs. $t^{0.65}$ increases rapidly first and then slowly.

Accepted Manuscript
Version of record at: https://doi.org/10.1088/1361-6528/aca76f

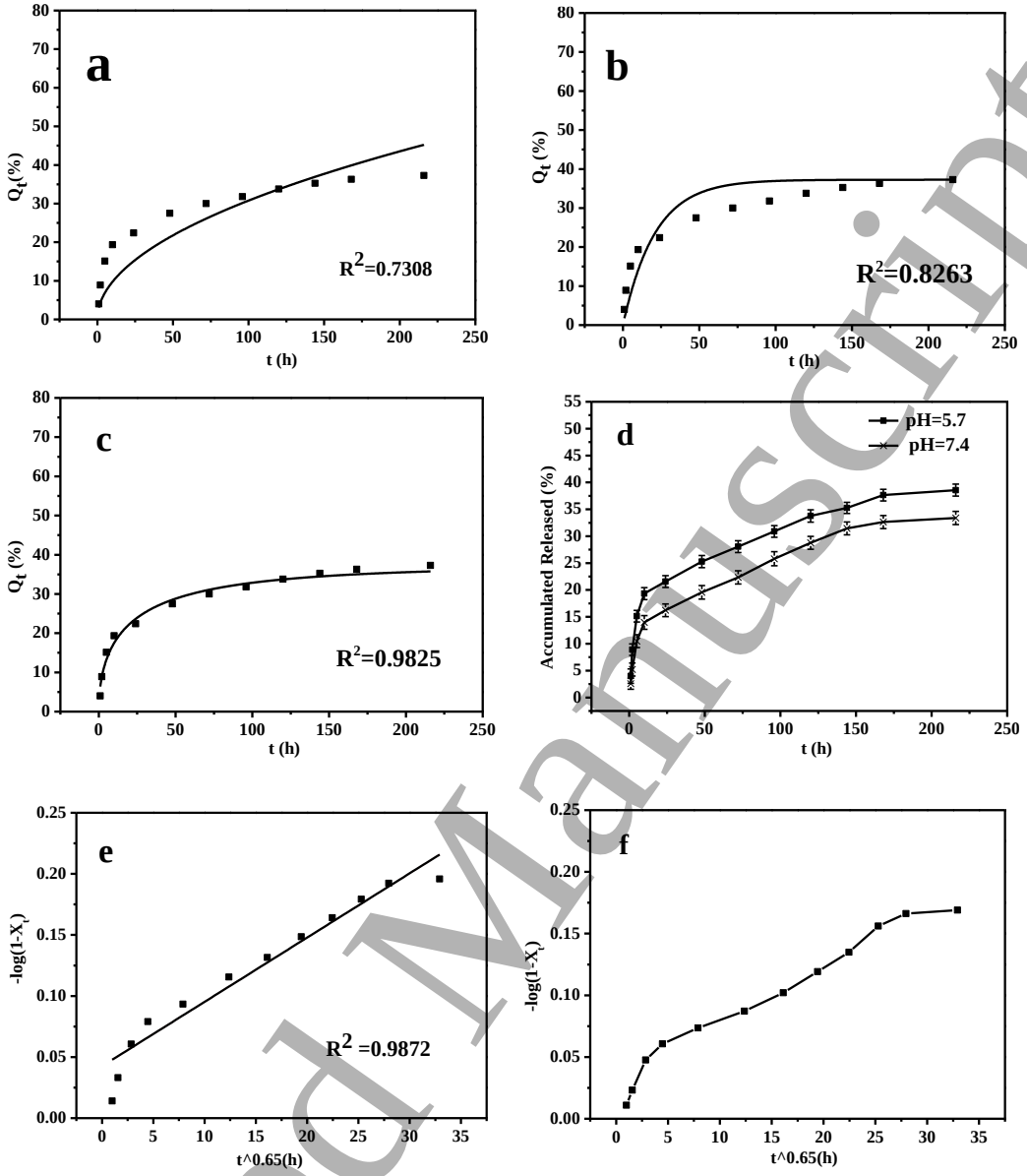

Fig.7 (a) Higuchi kinetic curve, (b) First-order kinetic curve and (c) Weibull kinetic curve ; (d) Sustained release rate of HMNPs@PDA-GQDs-FA to GA under different pH; Release

3.3 Studies on cytotoxicity

A further exploration on cytotoxicity and the targeting effect of FA on VX2 cells was made by MTT cell assay in this study. Various concentrations of HMNPs-GQDs, HMNPs@PDA-GQDs and HMNPs@PDA-GQDs-FA were first used to co-incubate with VX2 cells for 24 hours, where the cell viability was still above 95%, as shown in Fig. 8a. This indicates that synthesized HMNPs-GQDs, HMNPs@PDA-GQDs and

AUTHOR SUBMITTED MANUSCRIPT - NANO-132982.R3
Accepted Manuscript
Version of record at: https://doi.org/10.1088/1361-6528/aca76f

HMNPs@PDA-GQDs-FA have good biocompatibility and low toxicity to tissues and cells. After incubation with VX2 cells for 24 hours, HMNPs-GQDs(GA), HMNPs@PDA-GQDs(GA) and HMNPs@PDA-GQDs-FA(GA) of different concentrations show better cell growth inhibition in vitro compared to the carriers of unloaded GA. As shown in Fig. 8b, the survival rate of VX2 cells that incubated with HMNPs@PDA-GQDs-FA is 25.09±1.23% and with HMNPs@PDA-GQDs is 30.87±1.21%. This is because FA has targeting properties, and more drug-loaded materials can reach tumor cells and release drugs to induce death of tumor cell. In addition, cell viability decreases with increasing concentration, indicating that the compound nanoparticles after drug loading are concentration dependent on cell toxicity. Statistical analysis suggests that, compared with HMNPs-GQDs(GA), HMNPs@PDA-GQDs-FA(GA) has strong lethality to VX2 cell and HMNPs@PDA-GQDs(GA) comes second. To further study the targeting characteristics of FA, the cytotoxicity of HMNPs@PDA-GQDs-FA to MCF-7 cells was tested. The survival rate of HMNPs@PDA-GQDs-FA incubated VX2 cells is lower because of the overexpression of FA in VX2 cells, as shown in Fig. 8d. Due to the low expression of folic acid in MCF-7 cells, compound nanoparticles HMNPs@PDA-GQDs-FA can enter VX2 cells more effectively and reduce cell survival rate, so it has better anti-tumor effect in vivo.

Accepted Manuscript
Version of record at: https://doi.org/10.1088/1361-6528/aca76f

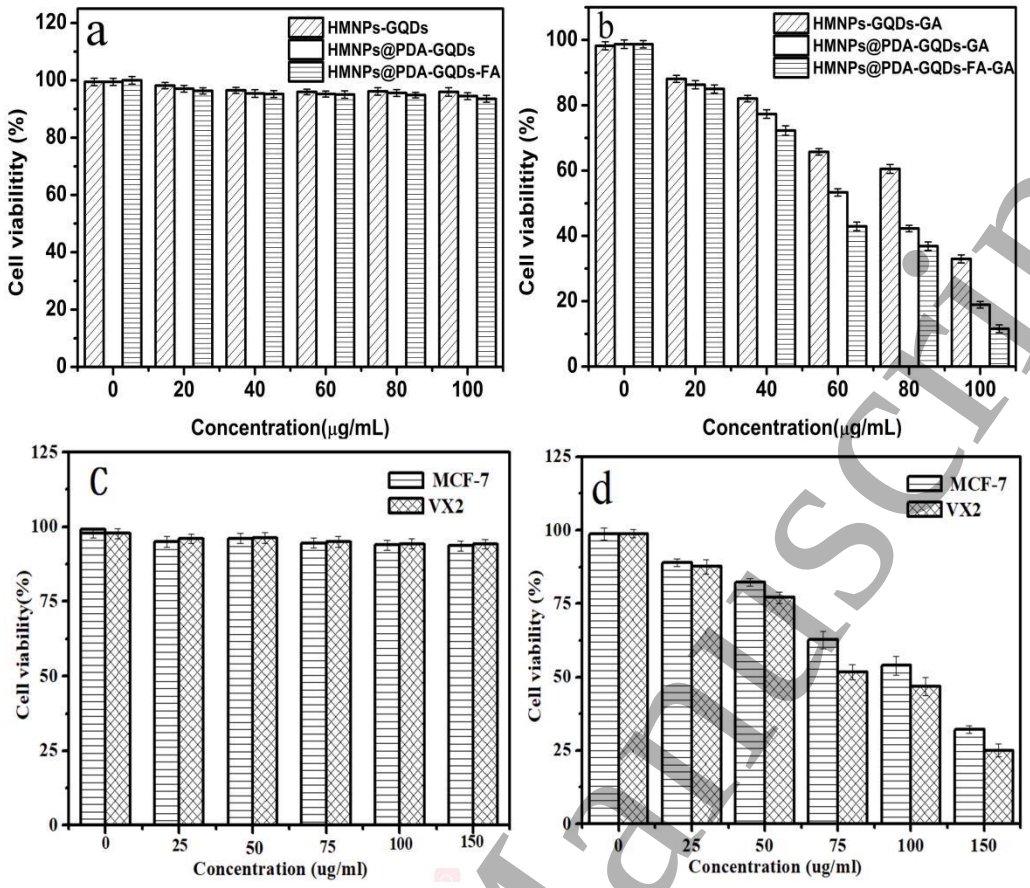

Fig.8 (a) and (b) MTT cytotoxicity assay analysis of VX2 cells treated with HMNPs-GQDs(GA), HMNPs@PDA-GQDs(GA) and HMNPs@PDA-GQDs-FA(GA) of different concentrations for 24h; (c) and (d) MTT cytotoxicity assay analysis of HMNPs@PDA-GQDs-FA(GA) on MCF-7 and VX2 cells

Figure 8 is HMNPs GQDs, HMNPs@PDA-GQDs, and HMNPs@PDA-GQDs-FA (represented by A, B and C respectively below) with different concentrations of unloaded GA, the result graph of VX2 cells' cytotoxicity, and the targeting effect of FA. In order to make the data more intuitive, we conducted a One-Way ANOVA analysis of the data obtained, as shown in the following table. $F_C > F_B > F_A > F_{crit}$, which shows that concentrations of unloaded GA have a significant impact on the cyclotoxicity of VX2 cells, and HMNPs@PDA-GQDs-FA has the greatest impact at 100 μg/ml with the strong lethality to VX2 cell reaching 88.42%.

AUTHOR SUBMITTED MANUSCRIPT - NANO-132982.R3
Accepted Manuscript
Version of record at: https://doi.org/10.1088/1361-6528/aca76f

This is due to the targeting capability of FA, more drug-loaded materials can reach tumor cells and release drugs to induce death of tumor cell.

Table 4 One-Way ANOVA: A, B and C with different concentrations of unloaded GA

A) HMNPs-GQDs

Source	SS	df	MS	F	P-value	F crit
Between groups	8217.2421	5	1643.4484	1233.9552	7.8261E-16	3.1058
Within group	15.9822	12	1.3318			
Total	8233.2243	17				

B) HMNPs@PDA-GQDs

Source	SS	df	MS	F	P-value	F crit
Between groups	13465.2117	5	2693.0423	1973.5513	4.7006E-17	3.1058
Within group	16.3748	12	1.3645			
Total	13481.5865	17				

C) HMNPs@PDA-GQDs-FA

Source	SS	df	MS	F	P-value	F crit
Between groups	16251.6860	5	3250.3372	1975.9089	4.6671E-17	3.1058
Within group	19.7398	12	1.6449			
Total	16271.4258	17				

To further explore the targeting of folic acid, the uptake extent of HMNPs@PDA-GQDs and HMNPs@PDA-GQDs-FA by cells was qualitatively investigated by confocal microscopy. Fig. 9 shows that fluorescence intensity can be detected after the incubation of HMNPs@PDA-GQDs and HMNPs@PDA-GQDs-FA with VX2 cells for 24h, which indicates that HMNPs@PDA-GQDs and HMNPs@PDA-GQDs-FA can enter the cells and reach the nucleus within 24 hours. The confocal images of HMNPs@PDA-GQDs and HMNPs@PDA-GQDs-FA

Accepted Manuscript
Version of record at: https://doi.org/10.1088/1361-6528/aca76f

co-incubated with VX2 cells are shown in Fig. 9a and b, respectively. It is noted that the fluorescence intensity of VX2 cells incubated with HMNPs-GQDs@PDA-FA is higher than that of cells cultured with HMNPs-GQDs@PDA, which is due to the higher cell absorption level of composite nanoparticles grafted with FA. Cells take up nanoparticle drug carriers through endocytosis, and the confocal microscopy shows that HMNPs@PDA-GQDs-FA nanoparticles has a targeting function, and FA can enhance cellular endocytosis through specific interactions with VX2 cells.

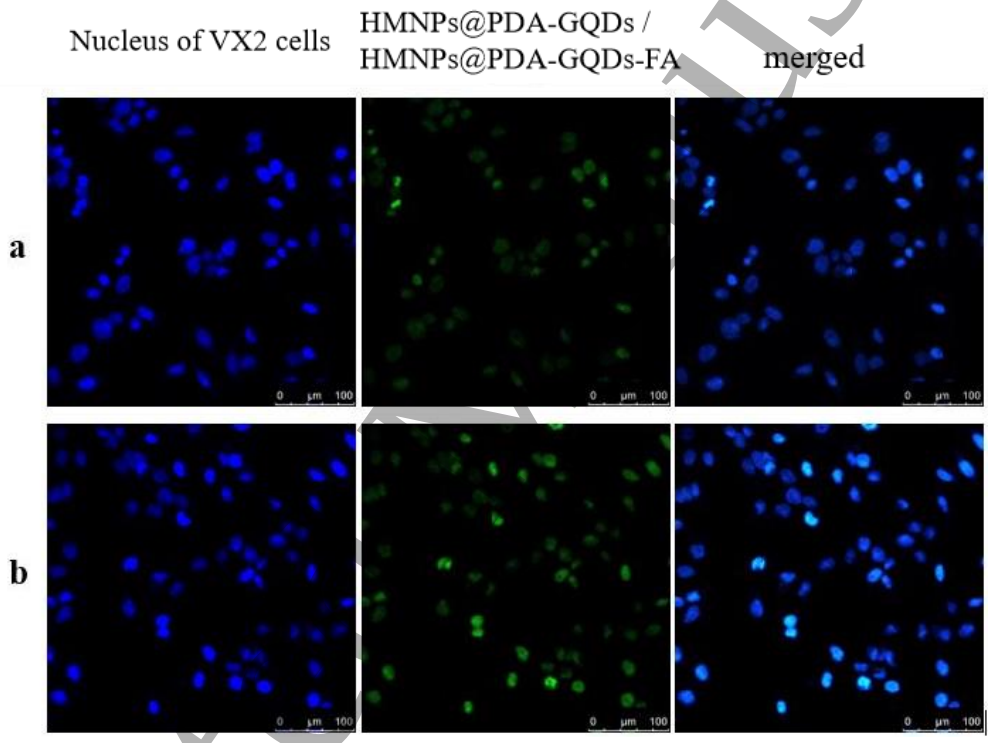

Fig.9 (a) HMNPs@PDA-GQDsand (b) HMNPs@PDA-GQDs-FA laser confocal fluorescence images of VX2 cells

To further investigate the critical role of FA in HMNPs-GQDs@PDA-FA cell uptake, experiments with different cells were conducted. Fig. S2 a and b show the confocal laser fluorescence images of MCF-7 and VX2 cells with the same amount of composite nanoparticle solution, where the VX2 fluorescence intensity of the cells is noticeably stronger due to higher uptake. The result suggests that the

AUTHOR SUBMITTED MANUSCRIPT - NANO-132982.R3
Accepted Manuscript
Version of record at: https://doi.org/10.1088/1361-6528/aca76f

HMNPs-GQDs@PDA-FA has a targeting function and FA can enhance HMNPs-GQDs@PDA-FA endocytosis by specific interactions with VX2 cells, which is consistent with the results of cytotoxicity experiments.

To study the inhibitory effect of HMNP@PDA-GQDs and HMNPs@PDA-GQDs-FA on tumor cells after drug loading (GA) (0.5 mg/μL), the effect of two vectors on VX2 tumor cells was studied in tumor-bearing mice. Fig. 10a shows the volume changes of tumor cells in the two groups after 28 days, where the inhibitory effect of HMNPs@PDA-GQDs-FA on tumor cells was more obvious. The tumor volume was only 30.1±1.23% of the initial tumor volume for HMNPs@PDA-GQDs-FA，while HMNPs@PDA-GQDs was 47.8±1.05% of the initial tumor volume. The mice were sacrificed 28 days after administration, and the targeting group was taken out for section study. Fig. 10c shows the HE staining (Hematoxylin eosin staining method) of the tumor section under a 10×20 magnification light microscope. It can be seen that the tumor cells are cordlike strips.

Accepted Manuscript
Version of record at: https://doi.org/10.1088/1361-6528/aca76f

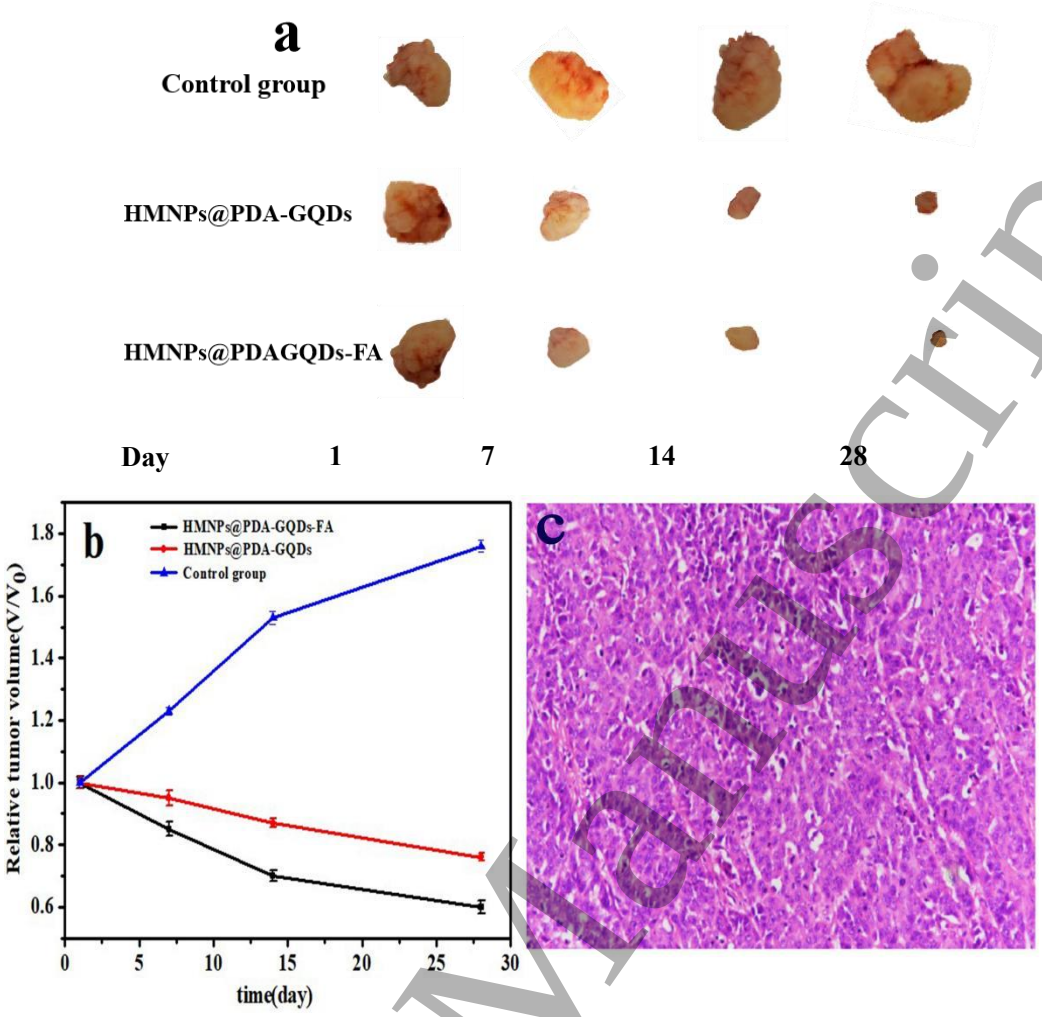

Fig. 10 (a) Tumor picture, (b) Growth of VX2 tumors after various treatments, (c) VX2 cell transplanted tumor section

3.4 Bio-distribution of magnetic silica nanoparticles in mice in vivo

To study the in vivo distribution of the magnetic nanoparticles in a variety of tissues, the female mice were selected as animal model. $^{99}Tc^{m}$ labelled radioactive HMNPs@PDA-GQDs-FA nanoparticles were injected into two anaesthetized mice via caudal vein. The nanoparticles were then detected by the SPECT and γ-counter. The mice were sacrificed in batches at different time and then dissected. The blood, heart, lung, liver, spleen, pancreas, stomach, small intestine, large intestine, brain, muscle, and bone were accurately weighed. Quantitative analysis was carried out by using a γ-counter to test the radioactivity count of each organ in the mouse.

AUTHOR SUBMITTED MANUSCRIPT - NANO-132982.R3
Accepted Manuscript
Version of record at: https://doi.org/10.1088/1361-6528/aca76f

Table 3 Biological distribution of nano magnetic particles in mice（%ID/g）

viscera	15 min	30 min	60 min	120 min	180 min
Blood	1.5875	1.2589	1.5022	2.9037	2.1623
heart	1.4783	1.4577	2.5802	2.0638	1.6606
lung	0.3290	0.4109	0.3134	0.5542	0.4542
kidney	0.2356	0.4224	0.3873	0.4985	0.4389
liver	33.2680	43.4987	89.0189	121.0530	69.2404
spleen	1.0501	1.2987	2.5026	2.4305	2.4016
pancreas	0.4579	0.6523	0.7492	0.9104	0.7301
stomach	1.0501	1.2987	2.5026	2.4305	2.4016
small intestine	1.0322	1.1396	1.4989	1.9100	1.4606
large intestine	0.6234	0.8702	1.2101	1.6470	1.5329
brain	0.0625	0.0478	0.0801	0.1098	0.1294
muscle	0.2720	0.4012	0.3789	0.5002	0.4304
bone	0.4243	0.6234	0.7653	0.8902	0.7421

Nanomagnetic particle distribution (%ID): Nanoparticles are concentrated in the liver. At 120 min, the amount of aggregation reached 121.0530% ID/g, while the amount of aggregation in other parts was relatively small, indicating that the HMNPs@PDA-GQDs-FA Nanoparticles have a good targeting performance, can target the liver efficiently, and has little side effects on normal cells.

Finally, we believe that the impact HMNPs@PDA-GQDs-FA on the drug release rate of the carrier has two effects. On one hand, GA has poor water solubility and only contains one hydroxyl group and one carboxyl group. In a slightly acidic environment of tumor, its protonation degree is not high, so its release rate is low. On the other hand, some surface mesopores are blocked by surface grafted groups (such as

Accepted Manuscript
Version of record at: https://doi.org/10.1088/1361-6528/aca76f

GQD-FA) so that drugs cannot be fully released from the pores at a faster speed.

To improve HMNPs@PDA-GQDs-FA as drug carrier with controlled release rate, we have the following ideas:

(1) Take advantage of a synergistic effect of photothermal therapy and chemotherapy by means of encapsulating PDA, micro PDA nanoparticles and GA drugs together in mesoporous SiO_2, and then coat PDA outside the mesopore. These microspheres have high photo thermal conversion efficiency and high photo stability. After the microspheres are injected into the tumor bearing mice, they are immediately irradiated with near-infrared light at the tumor site. Due to the photothermal effect and diffusion to the cells, the loaded GA will be rapidly released, thus increasing the drug release rate. Therefore, the synergistic effect of photothermal therapy and chemotherapy of the material can accelerate cell apoptosis, enhance the drug release rate, and promote the therapeutic effect of cancer[36,37].

(2) By derivatizing GA, GA containing only one hydroxyl group and one carboxyl group can be changed into GA derivatives containing more groups (such as GA3 derivatives). GA derivatives not only improve activity and anti-cancer effect, but also are easier to be protonated under acidic conditions, which is conducive to drug release[38].

(3) By optimizing the synthesis method, mesoporous silica with more uniform pore size can be synthesized, which will make the release of drugs more controllable from tailored pore sizes and the system more conducive to the diffusion release of the whole drug[39].

AUTHOR SUBMITTED MANUSCRIPT - NANO-132982.R3
Accepted Manuscript
Version of record at: https://doi.org/10.1088/1361-6528/aca76f

4. Conclusion

The preparation, loading and release, and toxicity to cells of GA on HMNPs@PDA-GQDs-FA were systematically investigated. HMNPs@PDA-GQDs-FA(GA) can release the drug quickly within 24 hours and continue the release for up to 190 hours. The cumulative release of HMNPs@PDA-GQDs-FA was identified to be 33.39±2.13% at pH 7.4 and 38.56±1.95% at pH 5.7, respectively. This is beneficial for the release of drugs in the acidic microenvironment of tumors. Cytotoxicity analysis showed that the cell survival rate was about 95% when treated with HMNPs@PDA-GQDs-FA without GA, but the cell survival rate dramatically decreased to 25.09±1.23% after loading GA, indicating that the cytotoxicity of the carrier was very low. The laser confocal fluorescence images show that more HMNPs@PDA-GQDs-FA can be up-taken by tumor cells compared to HMNPs@PDA-GQDs, indicating that the FA exhibits targeting performance and it has better targeting ability to VX2 cells. The composite nanomaterials demonstrate high potentials in the application of cancer therapy.

Acknowledgments

This work was supported by the National Natural Science Foundation of China (20577010, 20971043), the Fundamental Research Funds for the Central Universities, and the Open Project Program of State Key Laboratory of Inorganic Synthesis and Preparative Chemistry, Jilin University.

Competing interests

The authors declare that they have no known competing financial interests or

Accepted Manuscript
Version of record at: https://doi.org/10.1088/1361-6528/aca76f

personal relationships that could have appeared to influence the work reported in this paper.

Funding

This work was supported by the National Natural Science Foundation of China (20577010, 20971043), and the Open Project Program of State Key Laboratory of Inorganic Synthesis and Preparative Chemistry, Jilin University.

References

[1] Xie Y., Lu W., Wang S., et al. Validation of the 12-gene predictive signature for adjuvant chemotherapy response in lung cancer. Clinical Cancer Research. 25(2019) 150. DOi: 10.1158/1078-0432.CCR-17-2543

[2] Allen S. W., Hayashi R. J., Jones S. J., et al. Development of electronic chemotherapy roadmaps for pediatric oncology patients. Journal of Pediatric Oncology Nursing. 35 (2018) 314-319. DOi: 10.1177/1043454218767876

[3] Sparano J. A., Gray R. J., Makower D. F., et al. Adjuvant chemotherapy guided by a 21-gene expression assay in breast cancer. New England Journal of Medicine. 379 (2018)111-121.DOi: 10.1056/NEJMoa1804710

[4] Bonner J. A., Harari P. M., Giralt J., et al. Radiotherapy plus cetuximab for squamous-cell carcinoma of the head and neck. New England Journal of Medicine. 354 (2006) 567-578. DOi: 10.1056/NEJMoa053422

[5] Overgaard M., Hansen P. S., Overgaard J., et al. Postoperative radiotherapy in high-risk premenopausal women with breast cancer who receive adjuvant chemotherapy. New England Journal of Medicine. 337 (1997) 949-955. DOi: 10.1056/NEJM199710023371401

AUTHOR SUBMITTED MANUSCRIPT - NANO-132982.R3
Accepted Manuscript
Version of record at: https://doi.org/10.1088/1361-6528/aca76f

[6] Brown P. D., Ballman K. V., Cerhan J. H., et al. Postoperative stereotactic radiosurgery compared with whole brain radiotherapy for resected metastatic brain disease: A multicentre, randomised, controlled, phase 3 trial. The Lancet Oncology. 18 (2017) 1049-1060. DOi: 10.1016/S1470-2045(17)30441-2.

[7] Nguyen Q. T., Tsien R. Y.. Fluorescence-guided surgery with live molecular navigation - a new cutting edge. Nature Reviews Cancer. 13 (2013) 653.DOi:

[8] P Couvreur, B. Kante, M. Roland, et al.Adsorption of antineoplastic drugs to polyalkylcyanoacrylate nanoparticles and their release in calf serum. Pharm. Sci. 68 (1979) 1521-1524.DOi: 10.1002/jps.2600681215

[9] Avedian, N., Zaaeri ,et al.PH-sensitive biocompatible mesoporous magnetic nanoparticles labeled with folic acid as an efficient carrier for controlled anticancer drug delivery.Journal of Drug Delivery Science and Technology. 44 (2018) 323-332.DOi: 10.1016/j.jddst.2018.01.006

[10] Blanco E, Shen H, Ferrari M. Principles of nanoparticle design for overcoming biological barriers to drug delivery. Nature Biotechnology, 2015, 33: 941-951.

[11] Truong NP, Whittaker MR, Mak CW, Davis TP. The importance of nanoparticle shape in cancer drug delivery. Expert Opin. Drug Deliv., 2015, 12 (1):129-142.

[12] Toy R, Peiris PM, Ghaghada KB, Karathanasis E. Shaping cancer nanomedicine: The effect of particle shape on the in vivo journey of nanoparticles. Nanomedicine (Lond), 2014, 9 (1): 121-134.

[13] Yang Y, Liu Y, Cheng C, Shi H, Yang H, Yuan H, Ni C. Rational design of GO modified Fe3O4/SiO2 nanoparticles with combined Rhenium-188 and Gambogic acid for magnetic target therapy. ACS Appl. Mater. Interfaces, 2017, 9 (34): 28195-28208.

Accepted Manuscript
Version of record at: https://doi.org/10.1088/1361-6528/aca76f

[14] Sharma G, Valenta D T, Altman Y, et al. Polymer particle shape independently influences binding and internalization by macrophages. Journal of controlled release, 2010, 147(3): 408-412.

[15] Desai P, Venkataramanan A, Schneider R, et al. Self-assembled, ellipsoidal polymeric nanoparticles for intracellular delivery of therapeutics. Journal of Biomedical Materials Research Part A, 2018, 106(7): 2048-2058.

[16] Meyer R A, Sunshine J C, Perica K, et al. Immunoengineering: Biodegradable Nanoellipsoidal Artificial Antigen Presenting Cells for Antigen Specific T-Cell Activation. Small, 2015, 11(13): 1519-1525.

[17] Guo Q. L., You Q. D., Wu Z. Q., et al. General gambogic acids inhibited growth of human hepatoma SMMC-7721 cells in vitro and in nude mice. Acta Pharmacologica Sinica.25 (2004) 769-774.DOi: 10.1016/S0898-6568(03)00096-2

[18] Wu Z. Q., Guo Q. L., You Q. D., et al. Gambogic acid inhibits proliferation of human lung carcinoma SPC-A1 cells in vivo and in vitro and represses telomerase activity and telomerase reverse transcriptase mRNA expression in the cells. Biological & Pharmaceutical Bulletin. 27 (2004) 1769-1774.DOi: 10.1248/bpb.27.1769

[19] Zhao L., Guo Q. L., You Q. D., et al. Gambogic acid induces apoptosis and regulates expressions of Bax and Bcl-2 protein in human gastric carcinoma MGC-803 cells. Biological & Pharmaceutical Bulletin. 27 (2004) 998-1003. DOi: 10.1248/bpb.27.998

[20]F. Angius, A. Floris, Liposomes and MTT cell viability assay: An incompatible affair. Toxicology in Vitro 29, 314-319 (2015). doi:http://dx.doi.org

[21] Yuling Liu, Yingchong Chen , Longfei Lin ,etc.Gambogic Acid as a Candidate for Cancer Therapy: A Review. International journal of nanomedicine. 15 (2020) 10385-10399.DOi:

AUTHOR SUBMITTED MANUSCRIPT - NANO-132982.R3
Accepted Manuscript
Version of record at: https://doi.org/10.1088/1361-6528/aca76f

10.2147/IJN.S277645

[22]X. J. Wang et al., Multifunctional graphene quantum dots for simultaneous targeted cellular imaging and drug delivery. Colloids and Surfaces B-Biointerfaces 122, 638-644 (2014). doi:http://dx.doi.org.

[23]] L. Zhang, J. Xia, Q. Zhao, L. Liu, Z. Zhang, Functional graphene oxide as a nanocarrier for controlled loading and targeted delivery of mixed anticancer drugs,Small 6 (2010) 537–544.

[24] Y.He,Y. Lin,H. Tang, D. Pang,Agraphene oxide-basedflfluorescent aptasensor for the turn-on detection of epithelial tumor marker mucin 1, Nanoscale 4 (2012) 2054–2059.

[25]J. J. Zhou, B. Duan, Z. Fang, J. B. Song, C. X. Wang, P. B. Messersmith and H. W. Duan, Adv. Mater., 2014, 26, 701–705.

[26]S. R. Zhu et al., Hierarchical core-shell SiO2@PDA@BiOBr microspheres with enhanced visible-light-driven photocatalytic performance. Dalton Transactions 46, 11451-11458 (2017).

[27]M. Liu, W. Q. Jiang, Q. Chen, S. Wang, Y. Mao, X. L. Gong, K. C.-F. Leung, J. Tian, H. J. Wang and S. H. Xuan, RSC Adv., 2016, 6, 29279–29287

[28]X. J. Wang et al., Multifunctional graphene quantum dots for simultaneous targeted cellular imaging and drug delivery. Colloids and Surfaces B-Biointerfaces 122, 638-644 (2014). doi:http://dx.doi.org.

[29]Z. C. Dai et al., Preparation and Biological Applications of Graphene Oxide Functionalized Water-Based Magnetic Fluids. Journal of Nanoscience and Nanotechnology 18, 735-742 (2018). doi:http://dx.doi.org

[30] Yang Y .X., Ying H. P., Shao J. G., et al. A study on effect of different template chain length on synthesis of mesoporous silica in acidic condition. Journal of the American Ceramic Society.

Accepted Manuscript
Version of record at: https://doi.org/10.1088/1361-6528/aca76f

90 (2007) 3460-3467.DOi: 10.1111/j.1551-2916.2007.01951.x

[31] Gohel M. C. , Panchal M. K. , Jogani V. V. Novel mathematical method for quantitative expression of deviation from the Higuchi model. Aaps Pharmscitech. 1 (2000) 43-48.DOi: 10.1208/pt010431

[32] Naiki H. , Nakakuki K. . First-order kinetic model of Alzheimer's beta-amyloid fibril extension in vitro. Laboratory Investigation. 74 (1996) 374-383.

[33] Kosmidis K., Argyrakis P. , Macheras P. . A reappraisal of drug release laws using Monte Carlo simulations: The prevalence of the Weibull function. Pharmaceutical Research. 20 (2003) 988-95.DOi: 10.1023/A:1024497920145

[34] R. Bhaskar, S.R.S. Murthy, B.D. Miglani, et al.Int. J. Pharm. 28(1986) 59-66.DOi: 10.1016/0378-5173(86)90147-X

[35] Dong L., Yan L., Hou W. G. , et al. Synthesis and release behavior of composites of camptothecin and layered double hydroxide. Journal of Solid State Chemistry. 183 (2010) 1811-1816.DOi: 10.1016/j.jssc.2010.05.035

[36] R. Wu *et al.*, A photosensitizer-loaded zinc oxide-polydopamine core-shell nanotherapeutic agent for photodynamic and photothermal synergistic therapy of cancer cells. *Chin. Chem. Lett.* 31 (2020) 189-192. doi:http://dx.doi.org.

[37] S.S. Li *et al.*, Emulsifying performance of near-infrared light responsive polydopamine-based silica particles to control drug release. *Powder Technol.* **359** (2020) 17-26. doi:http://dx.doi.org.

[38]S. Y. Zhu, F. Z. Luo, P. H. Sun, Synthesis and antitumor activity of novel gibberellin derivatives with tetracyclic diterpenoid skeletons. *Med. Chem. Res.* **29** (2020) 1341-1354 . doi:http://dx.doi.org

AUTHOR SUBMITTED MANUSCRIPT - NANO-132982.R3
Accepted Manuscript
Version of record at: https://doi.org/10.1088/1361-6528/aca76f

[39]Z. Zhou *et al.*, Tailored ordered porous alumina with well-defined and uniform pore-structure.

Chem. Eng. J. 223 (2013) 670-677. doi:http://dx.doi.org)